Chapter 3

ELECTROCATALYSIS OF THE HYDROGEN-EVOLUTION REACTION BY ELECTRODEPOSITED AMORPHOUS COBALT SELENIDE FILMS

Carim, A. I.; **Saadi, F. H.**; Soriaga, M. P.; Lewis, N. S. *Journal of Materials Chemistry A* **2014**, *2*, 13835. DOI: 10.1039/C4TA02611J

3.1 Introduction

Our work in Chapter 2 focused on a simple wet chemical synthesis of catalytic molybdenum selenide which resulted in a mesoporous structure that exhibited overpotentials of ~250 mV for HER current densities of -10 mA cm^{-2}. In this chapter we extend our exploration of acid stable hydrogen evolution catalysts to cobalt chalcogenides.

The binary Co chalcogenides have not been investigated as thoroughly as their Mo analogues for catalysis of the HER, but several catalytically active preparations have been reported.[1-4] Nanocrystalline thin films of CoS_2 and $CoSe_2$ synthesized by treating metallic Co films with S vapor at 550 ˚C or Se vapor at 450 ˚C have achieved a current density of -4 mA cm^{-2} at overpotentials of ~ 220 mV and 200 mV, respectively, in N_2-dearated 0.5 M H_2SO_4. Nanoparticle films of $CoSe_2$ fabricated by treating CoO nanoparticles (initially formed by pyrolysis of an ink containing $Co(NO_3)\cdot 6H_2O$ at 600 ˚C) with Se vapor at 450 ˚C required an overpotential of ~ 210 mV to effect a current

density of -10 mA cm^{-2} in 0.5 M H_2SO_4. Amorphous films of Co-S, composed of Co and S in a ~ 1 : 1.4 atomic ratio, produced via electrodeposition followed by thermal annealing at 300 ˚C required an overpotential of ~ 160 mV to reach -10 mA cm^{-2} in phosphate buffer at pH = 7, but rapidly deactivated in 0.5 M H_2SO_4. Ni/NiO/$CoSe_2$ nanocomposites fabricated utilizing several hydrothermal, solvothermal, and annealing steps at temperatures between 180 and 250 ˚C have been shown to reach -10 mA cm^{-2} with an overpotential < 100 mV in Ar-saturated 0.5 M H_2SO_4, but are unstable in such media. Methods that employ solution-based techniques for catalyst synthesis and assembly under ambient conditions are preferable to high temperature and/or vapor-based techniques because solution-based techniques require relatively low energy inputs and provide increased compatibility with substrates. We describe herein an electrochemical method for the preparation of catalytically active, amorphous cobalt selenide films, from fully oxidized precursors in aqueous solution under ambient conditions.

3.2 Cobalt selenide electrodeposition and characterization

The cobalt selenide films were electrodeposited from an aqueous solution of $Co(C_2H_3O_2)_2$ and SeO_2 using potentiostatic electrolysis, and were then conditioned in 0.500 M H_2SO_4 using galvanostatic electrolysis in the HER regime (see section 3.5 for experimental methods). The cobalt selenide films were characterized by scanning electron microscopy (SEM), energy-dispersive X-ray spectroscopy (EDS), Raman spectroscopy, powder X-ray diffraction (XRD), and X-ray photoelectron spectroscopy (XPS).[5, 6] Figure 3.1A shows a scanning-electron micrograph of an electrochemically

prepared film. The films were mesoporous and contained pores estimated to be ~ 20 nm in diameter. Measurements made using EDS indicated a Co:Se atomic ratio of 1:2. The Raman spectra (Figure 3.1B) displayed no signatures of crystalline $CoSe_2$ nor of Se,[7, 8] but contained a broad band centered at ~ 233 cm^{-1} indicative of the stretching of Se–Se bonds in glassy selenium comprised of close-packed chains in which the local microscopic structure resembles that of crystalline, trigonal Se.[9] The Raman spectra also exhibited a less intense, lower frequency feature, centered at ~ 166 cm^{-1}, consistent with expectations for the bending of the Se–Se bonds in the close-packed chains as well as the presence of disordered CoSe.[10, 11]

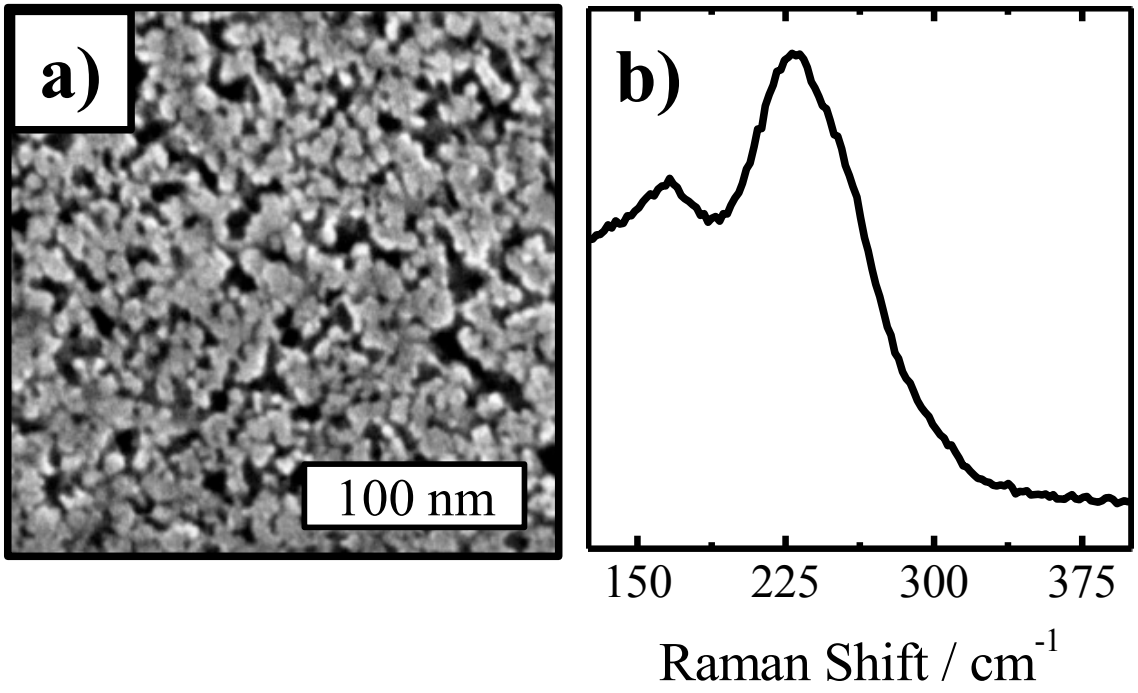

Figure 3.1: Representative (A) scanning electron micrograph and (B) Raman spectrum of an electrochemically prepared cobalt selenide film.

No signals were observed from oxygenated cobalt species.[12-14] The Raman spectra were consistent with the XRD pattern obtained for the film (Figure 3.2), which only exhibited reflections that corresponded to the Ti substrate and did not show reflections that corresponded to any crystalline cobalt selenide species.

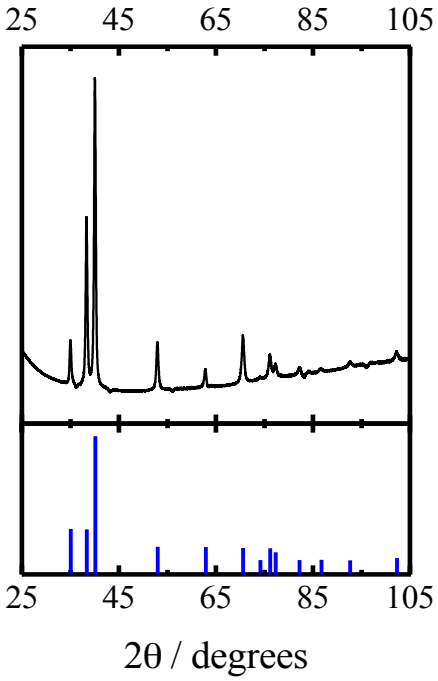

Figure 3.2: Top: Representative X-ray diffraction pattern collected from a cobalt selenide film. Bottom: Standard lines for polycrystalline Ti (JCPDS 65-9622).

High-resolution XPS analysis of the Co 2p region (Figure 3.3A) displayed an intense Co $2p_{3/2}$ line at 781.5 eV which was not consistent with expectations for $CoSe_2$.[15] XPS analysis of the Se 3d region (Figure 3.3B) revealed the presence of Se in both the Se^0 and Se^{2-} oxidation states. Thus, the cumulative data suggest that the films were composed of disordered CoSe in a polymeric Se matrix.

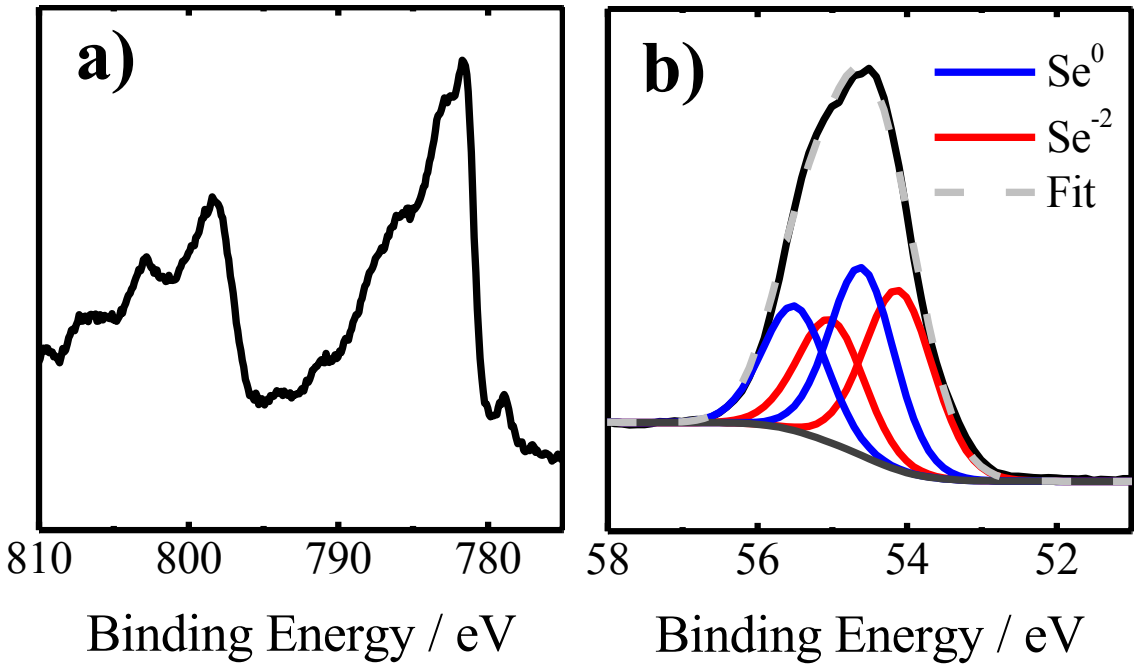

Figure 3.3: Representative high-resolution X-ray photoelectron spectra of an electrochemically prepared cobalt selenide film in the (A) Co 2p and (B) Se 3d regions.

Figure 3.4A presents the cathodic polarization behavior of a cobalt selenide film, as well as that of a bare titanium substrate, in a three-electrode voltammetric configuration in an aqueous solution of 0.500 M H_2SO_4 that was saturated with 1 atm of H_2 (g). The overpotentials required to produce current densities of -10 mA cm^{-2} and -25 mA cm^{-2} at a cobalt selenide film were 135 ± 2 mV and 160 ± 3 mV (mean ± s.d.), respectively, based on six independently prepared films. The Ti substrate exhibited negligible current densities throughout the interrogated potential window. Titanium is an ineffective HER catalyst and thus provides a clean background for interrogating the HER activity of other materials. Figure 3.4B presents a Tafel plot (overpotential versus log [|current density|]) derived from the voltammetric data of Figure 3.4A. A Tafel slope of

62 mV dec^{-1} and an exchange current density of 6.4 x 10^{-2} mA cm^{-2} were derived from the region between 110 and 180 mV in overpotential. The 62 mV dec^{-1} Tafel slope is inconsistent with the predicted values for the HER in acidic solution at room temperature characteristic of the Volmer (~ 120 mV dec^{-1}), Heyrovsky (~ 40 mV dec^{-1}) or Tafel (~ 30 mV dec^{-1}) elementary reactions.[16, 17] Slopes of ~ 60 mV dec^{-1} may be observed when either the Heyrovsky or the Tafel reaction is rate-limiting if the adsorption of hydrogen atoms onto the electrode requires an activation energy.[18] The ~ 60 mV dec^{-1} Tafel slope is consistent with the value observed for several amorphous molybdenum sulfide catalysts.[5, 6]

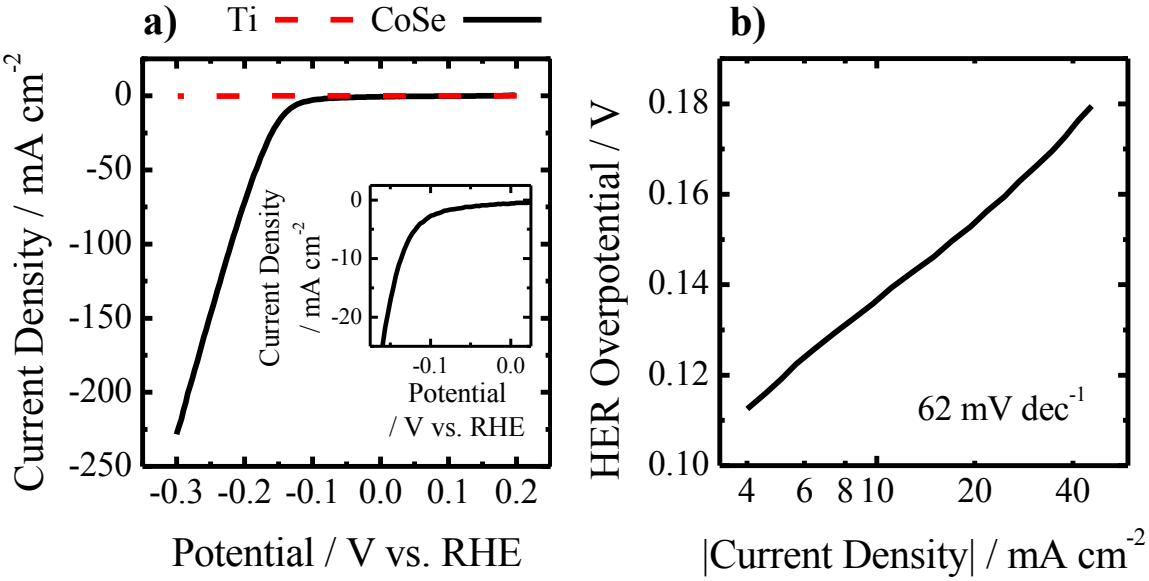

Figure 3.4: (A) Cathodic polarization curves of titanium foil and of a cobalt selenide film in 0.500 M H2SO4 saturated with H2(g) (inset highlights behavior at low overpotentials). (B) Tafel plot derived from data in (A).

Turnover frequencies (TOFs) exhibited by the cobalt selenide films for the HER were derived from the voltammetric data by a method previously reported for an amorphous molybdenum sulfide film (see the experimental section for calculation details).[6] A plot of the TOF as a function of HER overpotential is presented in Figure 3.5. TOF values were estimated to be 1 s^{-1} at an overpotential of 100 mV and of 5 s^{-1} at an overpotential of 150 mV.

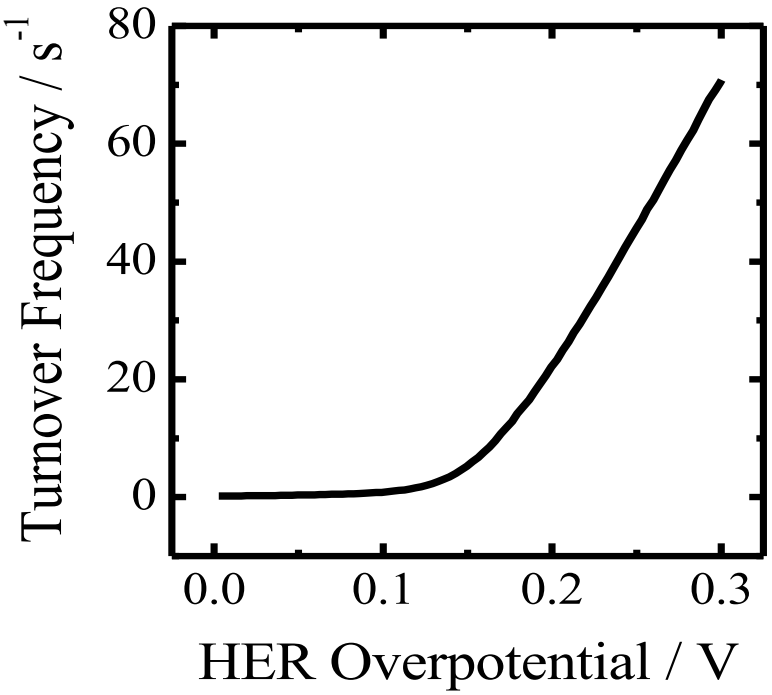

Figure 3.5: Turnover frequency of cobalt selenide films as function of overpotential for the hydrogen-evolution reaction in 0.500 M $H2_SO_4$ saturated with H_2(g) derived from the voltammetric data in Figure 3.4A.

The stability of the as-prepared CoSe films during electrochemical hydrogen evolution was assessed by two independent experimental protocols. First, a current

density of -10 mA cm^{-2} was maintained galvanostatically and the electrode potential was monitored as a function of time (Figure 3.6A). Over 16 h of continuous operation, the overpotential required to maintain this current density increased by ~ 5 mV. Separately, an accelerated degradation study[3, 19] was performed wherein the electrode potential was swept repeatedly between 0.100 and -0.175 V vs. RHE for 1000 full cycles. Voltammograms recorded before and after cycling (Figure 3.6B) revealed that the overpotential required to achieve current densities of -10 mA cm^{-2} and -25 mA cm^{-2} increased by less than 5 mV in both cases. The catalytic stability of the CoSe films during the HER in 0.5 M H_2SO_4 is consistent with that displayed by polycrystalline cobalt diselenide films prepared by treating metallic cobalt films with Se vapor, but is in contrast to that displayed by electrodeposited amorphous Co-S films which quickly dissolve under these conditions.[2, 3] These observations are consistent with the fact that in solutions with pH < 4, Se is cathodically stable until at least -0.4 V vs. RHE, whereas the reduction of S to H_2S is thermodynamically possible at potentials > 0 V vs. RHE.[20]

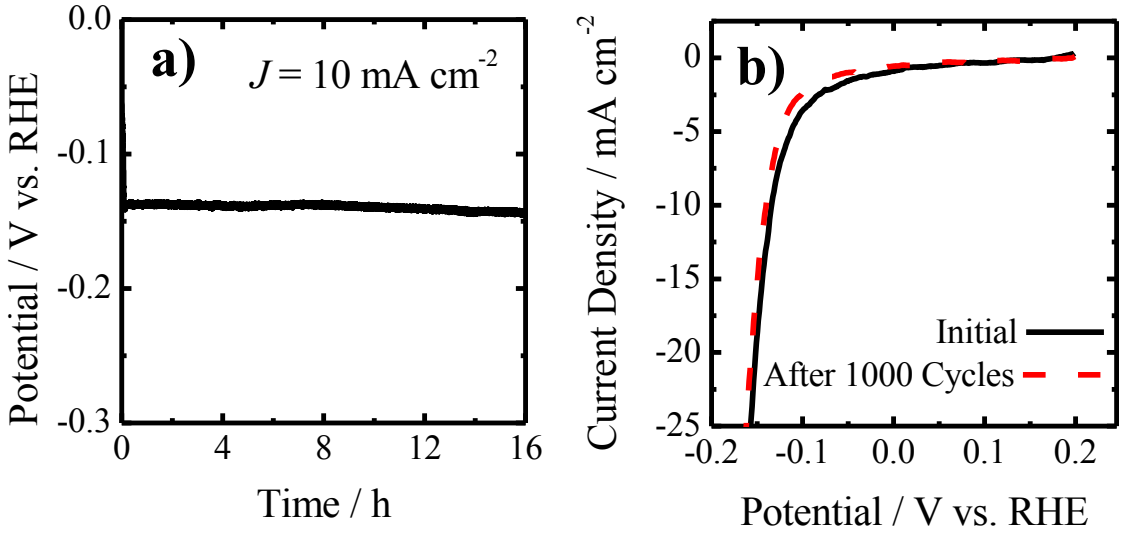

Figure 3.6: (A) Potential applied to a cobalt selenide film as a function of time during galvanostatic electrolysis at -10 mA cm-2 in 0.500 M H2SO4 (B) Polarization curves of a cobalt selenide film acquired before and after 1000 accelerated full potential cycles between 0.100 V and -0.175 V vs. RHE.

3.3 Comparison with other HER Catalysts

The ~ 135 mV overpotential for effecting current densities of -10 mA cm^{-2} in 0.500 M H_2SO_4 exhibited by the cobalt selenide films described in this work compares well to the values for other stable and highly-active catalyst materials in acidic media that are composed of Earth-abundant elements. Defective and disordered ultrathin nanosheets of MoS_2 as well as nanosheets of the 1T-MoS_2 polymorph have been demonstrated to achieve -10 mA cm^{-2} with overpotentials in the range of 180 – 190 mV.[21-23] MoS_2/reduced graphene oxide composites have reached current densities of -10 mA cm^{-2} with an overpotential of ~ 160 mV.[19] Ni_2P nanoparticles have been shown to drive

current densities of -10 mA cm^{-2} with an overpotential of ~ 120 mV.[24] Notably, the cobalt selenide films described herein were prepared entirely at room temperature and ambient conditions, via a facile electrochemical method. As synthesized, the amorphous Se matrix containing the CoSe may not act as a good electrical conductor, so the activity reported in this work may represent a lower bound on the true electrocatalytic activity of the material.[25] Additionally, Mo_2C supported on carbon nanotubes and amorphous MoS_x coated on N-doped carbon nanotubes have been shown to effect current densities of -10 mA cm^{-2} with overpotentials of ~ 150 mV and 110 mV, respectively.[26, 27] Similarly, nanoparticles of $CoSe_2$ have achieved -10 mA cm^{-2} with an overpotential of 137 mV when deposited on a high-surface area, porous, three-dimensional electrode (carbon fiber paper).[4] Fabrication of a similar structured composite with electrochemically prepared cobalt selenide may thus lead to improved performance. Similarly, deposition with dynamic potential-time waveforms, as well as alloying with Fe or Ni as has been done to promote the activity of molybdenum sulfide, could also prove effective for increasing the activity of cobalt selenide-based materials.[28, 29]

3.4 Conclusion

In conclusion, cobalt selenide films prepared by a simple electrochemical method under ambient conditions have demonstrated significant electrocatalytic activity and stability for catalysis of the HER in strongly acidic aqueous solution. This work suggests that electrochemically synthesized metal chalcogenide materials are promising catalysts for applications involving the HER, especially for applications involving the direct

production of fuels from sunlight in solar-driven water splitting systems.[30, 31] Moreover, investigations of deposition on structured supports, complex potential-time waveforms for electrodeposition, and alloying with other transition metals, as have been demonstrated for MoS_2, may result in further enhancements of the HER activity of such materials.[5, 32]

3.5 Experimental

Materials and Chemicals: H_2(g) (99.999%, Air Liquide), H_2SO_4 (J.T. Baker, A.C.S. Reagent), Ti foil (99.7+%, 0.127 mm thick, Sigma-Aldrich), SeO_2 (99.999%, Acros Organics), $Co(C_2H_3O_2)_2 \cdot 4H_2O$ (98%, Strem Chemicals) and LiCl (≥ 99.0%, Sigma-Aldrich) were used as received. H_2O with a resistivity ≥ 18.2 MΩ cm^{-1} (Barnsted Nanopure System) was used throughout.

Cobalt Selenide Electrodeposition: Cobalt selenide films were prepared on Ti substrates via electrodeposition. The sealed, single-compartment electrochemical cell equipped was with a graphite-rod counter electrode (Alfa Aesar, 99%) and a Ag/AgCl reference electrode (3 M KCl; Bioanalytical Systems) that were collectively controlled by a Bio-Logic SP-200 potentiostat. Squares ~ 2 cm x 2 cm in dimension were cut from the Ti foil and were then sealed into an O-ring compression cell that confined the contact region between the electrolyte, an aqueous solution of 0.065 M $Co(C_2H_3O_2)_2$, 0.035 M SeO_2 and 0.200 M LiCl (pH = 4.7), and the Ti foil, to a circular area of 0.1 cm^2. An external electrical contact to the Ti foil was made using an alligator clip. Electrodeposition was effected by potentiostatically biasing the Ti at a potential of -0.45

V vs. the Ag/AgCl reference electrode for 8 h at room temperature. After deposition, the Ti foil pieces were removed from the compression cell and rinsed first with 0.500 M H_2SO_4 and then with H_2O. The area of the Ti substrate that had not been covered by the electrodeposited cobalt selenide was then covered with nitrocellulose-based nail polish to provide electrical insulation.

Electrochemical Conditioning and Analysis: A single-compartment cell equipped with a graphite-rod counter electrode and a saturated calomel electrode (SCE; CH Instruments) and controlled by a Bio-Logic SP-200 potentiostat was used for conditioning and analysis of the electrodeposited material. An O-ring compression seal was used to mount the Ti substrate that supported the electrodeposited material in the cell. All experiments were performed using an aqueous solution of 0.500 M H_2SO_4 that was continuously sparged with H_2(g) and stirred using a magnetic stir bar. The potential of a reversible hydrogen electrode (RHE) relative to the SCE was determined by measuring the potential of a Pt foil (which was annealed in a H_2-air flame immediately prior to use) in the H_2(g)-saturated 0.500 M H_2SO_4 electrolyte. All quoted potentials are referenced against RHE unless otherwise noted. Prior to voltammetric experiments and physical characterization, electrodes were preconditioned by galvanostatic electrolysis at a current density of -10 mA cm^{-2} for 1 h. The CoSe mass loading was determined to be 3 mg cm^{-2}. The uncompensated cell resistance (R_u) was determined from a single-point electrochemical impedance measurement obtained by applying a sine-wave modulated potential with amplitude of 20 mV at a modulation frequency of 100 kHz centered at the open-circuit potential of the cell. All subsequent measurements were corrected for an uncompensated resistance of 85% of the value of R_u. Voltammetric data were recorded at

a scan rate of 1 mV s^{-1}. The electrochemical stability of the cobalt selenide films was assessed using both galvanostatic and accelerated degradation techniques. First, a current density of -10 mA cm^{-2} was maintained galvanostatically and the electrode potential was monitored over the course of 16 h. Separ ately, the cobalt selenide films were subjected to 1000 full potential cycles between -0.175 V and 0.1 V vs. RHE at a sweep rate of 50 mV s^{-1}. Voltammograms at a sweep rate of 1 mV s^{-1} were recorded before cycling and after completion of the 1000 full potential cycles.

Physical Characterization: Scanning electron microscopy (SEM) was conducted using a FEI Nova NanoSEM 450 at an accelerating voltage of 15 kV with a working distance of 5 mm and an in-lens secondary electron detector. Energy-dispersive X-ray spectroscopy was performed in the SEM at a working distance of 12 mm, using an accelerating voltage of 15 kV and an Oxford Instruments silicon drift detector. Raman spectra were obtained with a Renishaw inVia spectrometer equipped with a Leica microscope, a Leica N Plan 50x objective (numerical aperture = 0.75), an 1800 lines mm^{-1} grating, and a CCD detector in a 180˚ backscatter geometry. A 532 nm diode-pumped solid state (DPSS) laser (Renishaw RL532C50) was used as the excitation source and a radiant power of 20 μW was incident on the sample. X-ray diffraction (XRD) powder patterns were acquired with a Bruker D8 Discover diffractometer equipped with a Cu Kα source and a 2-dimensional Vantec detector. X-ray photoelectron spectra (XPS) were acquired with a Kratos Axis Nova spectrometer at a base pressure of 10^{-9} torr with monochromatic Al Kα excitation at 1486.7 eV. High-resolution spectra were obtained using a pass energy of 40 eV. CasaXPS software (CASA Ltd) was used to fit peaks in the XP spectra, and peak fitting was performed assuming a Shirley background and

symmetric Voigt line-shapes comprised of Gaussian (70%) and Lorentzian (30%) functions. The peak fitting was constrained to maintain both a 2:3 ratio between the areas of the Se $3d_{3/2}$ and Se $3d_{5/2}$ lines and to maintain a 0.85 eV separation between the binding energies of these two lines.

Calculation of turnover frequencies: Turnover frequencies of the cobalt selenide films for the hydrogen-evolution reaction were calculated the method previously reported for an amorphous molybdenum sulfide catalyst film.[35] The number of surface sites per unit area was estimated by calculating the area occupied by a CoSe unit in freboldite to determine the number of surface sites for a planar material and then scaling this value by the roughness factor of the cobalt selenide film (13, determined via electrochemical capacitance measurements). The selenium-selenium distance in frebdolite is 0.361 nm. Based on the arrangement of selenium atoms in the frebdolite basal plane, each Se atom, and thus each CoSe unit, occupies 0.13 nm^2. Thus, freboldite has approximately 8×10^{14} surface sites per cm^2 in the basal plane. From this, it is estimated that the cobalt selenide films had approximately 1×10^{16} surface sites per cm^2. The total number of hydrogen evolution turnovers was analytically derived from the current density via the conversion factor 3.1×10^{15} H_2 s^{-1} mA^{-1}. The turnover frequency is then the total number of turnovers divided by the number of active sites. Figure 3.5 presents a plot of turnover frequency as function of hydrogen-evolution reaction overpotential derived from the data in Figure 3.4A.

3.6 References

1. Y. F. Xu, M. R. Gao, Y. R. Zheng, J. Jiang and S. H. Yu, *Angew. Chem. Int. Ed.*, 2013, **52**, 8546-8550.

2. Y. Sun, C. Liu, D. C. Grauer, J. Yano, J. R. Long, P. Yang and C. J. Chang, *J. Am. Chem. Soc.*, 2013, **135**, 17699-17702.

3. D. Kong, J. J. Cha, H. Wang, H. R. Lee and Y. Cui, *Energy Environ. Sci.*, 2013, **6**, 3553.

4. D. Kong, H. Wang, Z. Lu and Y. Cui, *J. Am. Chem. Soc.*, 2014, **136**, 4897-4900.

5. D. Merki, S. Fierro, H. Vrubel and X. Hu, *Chem. Sci.*, 2011, **2**, 1262.

6. J. D. Benck, Z. Chen, L. Y. Kuritzky, A. J. Forman and T. F. Jaramillo, *ACS Catal.*, 2012, **2**, 1916-1923.

7. E. Anastassakis, *Solid State Commun.*, 1973, **13**, 1297-1301.

8. G. Lucovsky, A. Mooradian, W. Taylor, G. B. Wright and R. C. Keezer, *Solid State Commun.*, 1967, **5**, 113-117.

9. S. N. Yannopoulos and K. S. Andrikopoulos, *J. Chem. Phys.*, 2004, **121**, 4747-4758.

10. S. N. Yannopoulos and K. Andrikopoulos, *Phys. Rev. B*, 2004, **69**, 114206.

11. C. E. M. Campos, J. C. de Lima, T. A. Grandi, K. D. Machado and P. S. Pizani, *Physica B*, 2002, **324**, 409-418.

12. V. G. Hadjiev, M. N. Iliev and I. V. Vergilov, *J. Phys. C Solid State*, 1988, **21**, L199-L201.

13. D. Gallant, M. Pézolet and S. Simard, *J. Phys. Chem. B*, 2006, **110**, 6871-6880.

14. J. Tyczkowski, R. Kapica and J. Łojewska, *Thin Solid Films*, 2007, **515**, 6590-6595.

15. H. van der Heide, R. Hemmel, C. F. van Bruggen and C. Haas, *J. Solid State Chem.*, 1980, **33**, 17-25.

16. N. Pentland, J. O. Bockris and E. Sheldon, *J. Electrochem. Soc.*, 1957, **104**, 182-194.

17. B. E. Conway and B. V. Tilak, *Electrochim. Acta*, 2002, **47**, 3571-3594.

18. J. G. N. Thomas, *Trans. Faraday Soc.*, 1961, **57**, 1603-1611.

19. Y. Li, H. Wang, L. Xie, Y. Liang, G. Hong and H. Dai, *J. Am. Chem. Soc.*, 2011, **133**, 7296-7299.

20. M. Pourbaix, Atlas of Electrochemical Equilibria In Aqueous Solutions, Permagon Press, Oxford, 1966.

21. J. Xie, H. Zhang, S. Li, R. Wang, X. Sun, M. Zhou, J. Zhou, X. W. Lou and Y. Xie, *Adv. Mater.*, 2013, **25**, 5807-5813.

22. J. Xie, J. Zhang, S. Li, F. Grote, X. Zhang, H. Zhang, R. Wang, Y. Lei, B. Pan and Y. Xie, *J. Am. Chem. Soc.*, 2013, **135**, 17881-17888.

23. M. A. Lukowski, A. S. Daniel, F. Meng, A. Forticaux, L. Li and S. Jin, *J. Am. Chem. Soc.*, 2013, **135**, 10274-10277.

24. E. J. Popczun, J. R. McKone, C. G. Read, A. J. Biacchi, A. M. Wiltrout, N. S. Lewis and R. E. Schaak, *J. Am. Chem. Soc.*, 2013, **135**, 9267-9270.

25. K. E. Murphy, B. B. Wunderlich and B. Wunderlich, *J. Phys. Chem.*, 1982, **86**, 2827-2835.

26. W. F. Chen, C. H. Wang, K. Sasaki, N. Marinkovic, W. Xu, J. T. Muckerman, Y. Zhu and R. R. Adzic, *Energy Environ. Sci.*, 2013, **6**, 943.

27. D. J. Li, U. N. Maiti, J. Lim, D. S. Choi, W. J. Lee, Y. Oh, G. Y. Lee and S. O. Kim, *Nano Lett.*, 2014, **14**, 1228-1233.

28. D. Merki, H. Vrubel, L. Rovelli, S. Fierro and X. Hu, *Chem. Sci.*, 2012, **3**, 2515.

29. X.-J. Lv, G.-W. She, S.-X. Zhou and Y.-M. Li, *RSC Advances*, 2013, **3**, 21231.

30. S. Haussener, C. Xiang, J. M. Spurgeon, S. Ardo, N. S. Lewis and A. Z. Weber, *Energy Environ. Sci.*, 2012, **5**, 9922.

31. J. R. McKone, N. S. Lewis and H. B. Gray, *Chem. Mater.*, 2014, **26**, 407-414.

32. Z. Chen, D. Cummins, B. N. Reinecke, E. Clark, M. K. Sunkara and T. F. Jaramillo, *Nano Lett.*, 2011, **11**, 4168-4175.